Res Nondestr Eval (2000) 12:17–30

DOI: 10.1007/s001640000002

Nonlinear Elastic Wave Spectroscopy (NEWS) Techniques to Discern Material Damage, Part I: Nonlinear Wave Modulation Spectroscopy (NWMS)

K. E.-A. Van Den Abeele,[1] P. A. Johnson,[2] A. Sutin[3]

[1]Department of Building Physics, Catholic University Leuven, B-3001 Heverlee, Belgium
[2]Los Alamos National Laboratory, Los Alamos, NM 875454, USA
[3]Stevens Institute of Technology, Hoboken, NJ 07030, USA

Abstract. The level of nonlinearity in the elastic response of materials containing structural damage is far greater than in materials with no structural damage. This is the basis for nonlinear wave diagnostics of damage, methods which are remarkably sensitive to the detection and progression of damage in materials. Nonlinear wave modulation spectroscopy (NWMS) is one exemplary method in this class of dynamic nondestructive evaluation techniques. The method focuses on the application of harmonics and sum and difference frequency to discern damage in materials. It consists of exciting a sample with continuous waves of two separate frequencies simultaneously, and inspecting the harmonics of the two waves, and their sum and difference frequencies (sidebands). Undamaged materials are essentially linear in their response to the two waves, while the same material, when damaged, becomes highly nonlinear, manifested by harmonics and sideband generation. We illustrate the method by experiments on uncracked and cracked Plexiglas and sandstone samples, and by applying it to intact and damaged engine components.

1. Introduction

Experimental evidence for the highly nonlinear behavior of microcracked and damaged materials has existed for years from experiments of static stress–strain behavior and dynamic nonlinear wave interaction, but the methodology has yet to be developed and applied for materials testing procedures, except in rare instances.

Nonlinear elastic wave spectroscopy (NEWS) methods are powerful new tools in interrogation of damage in materials. Due to material nonlinearity, a wave can distort, creating accompanying harmonics, multiplication of waves of different frequencies, and, under resonance conditions, changes in resonance frequencies as a function of drive amplitude. In undamaged materials, these phenomena are very weak. In damaged materials, they are remarkably large. The sensitivity of nonlinear methods to the detection of damage features (cracks, flaws, etc.) is far greater than that of linear acoustical methods (measures of wave speed and wave dissipation), and in fact, these methods appear to be more sensitive than *any* method currently available [1–12].

There are two general NEWS approaches to damage detection by nonlinear wave means. One NEWS method, nonlinear resonant ultrasound spectroscopy (NRUS), depends on the study of the nonlinear response of a single, or a group of, resonant modes within the material. Resonance frequency shifts, harmonics, and damping characteristics are analyzed as function of the resonance peak acceleration amplitude. The method is extremely useful for basic research and specific applications that do not have strict time requirements in terms of speed of application [14–16]. The simple-mode nonlinear resonant ultrasonic spectroscopy technique (SIMONRUS, a single-mode version of NRUS) and an application of this technique is addressed in Part II [17].

The method presented here is nonlinear wave modulation spectroscopy (NWMS). This method can be quickly applied, and in our view, is ideally suited to applications where the question of damaged versus undamaged must be addressed quickly. Fundamentally, NWMS is based on monitoring nonlinear wave mixing in the material. The manifestations of the nonlinear response appear as wave distortion and accompanying wave harmonics, and in sum and difference frequency generation (sidebands). The approach has proved to be time efficient and effective in discerning damage to materials in our experience [11–13].

Initially, microcracked materials undergoing structural damage show progressively enhanced features of nonlinear elastic response [11–13, 16, 17]. In undamaged materials such as intact aluminum, steel, or Plexiglas, the manifestations of nonlinear response are extremely small and difficult to measure. These materials respond with *atomic nonlinearity*, or deformation at the atomic/molecular scale. Their nonlinear behavior is well understood and well described by classical nonlinear acoustical perturbation theory [18, 19]. In the same materials when damaged, the nonlinear response and the manifestations of nonlinearity are very large and easy to measure [11–13, 16, 17, 20–23]. The large nonlinear response arises from the complex compliance of local or volumetric cracks that are mesoscale (10^{-9} m) and larger, entirely dominating the relatively small atomic nonlinearity. However, the nonlinear response is far more complicated than the cracks themselves, being also related to fluids in cracks and absorbed fluids on crack walls. The full mechanism of the nonlinear response is not yet well understood. Fortunately, however, application of NWMS does not require an understanding of the mechanism of nonlinearity. From various static and dynamic experiments we do know that microcracked materials cannot normally be described by classical theory. When damaged, intact materials become what we call *nonlinear mesocopic elastic* materials and have at least one of the following properties: they are highly nonlinear, and/or they exhibit hysteresis and discrete memory in their stress–strain relation [23]. The theoretical description of nonlinear mesoscopic elastic materials contains terms that describe classical nonlinearity, as well as hysteresis, and discrete memory [24–29]. Comparison between experimental data and theoretical simulations provides essential information as to what type of nonlinearity is dominant in the material. Qualitatively we can say that the more damaged a material is, the larger is its nonlinear response. The quantitative relationship has yet to be demonstrated, however.

In this paper we describe the NWMS method and provide examples from three different materials. Two of the materials, Plexiglas and an engine component, are intact materials that, when cracked, become nonlinear mesoscopic materials. The third material

is a sandstone. Sandstone is composed of atomic material bonded together by contacts that can be soft. This rock generally has numerous microcracks. Because of its architecture, it is nonlinear mesoscopic to begin with. When a crack is added, it becomes even more nonlinear, as will be illustrated. All these results indicate that the nonlinear response of the material when damaged is extremely large when compared to the intact material.

First, in order to interpret the experimental data in a meaningful way, we briefly review the current state of the art in dynamic modeling of nonlinear elasticity and acoustic wave interaction.

2. Theoretical Background

Various static and dynamic experiments imply that the dynamic elastic behavior of most solid materials cannot be described by a linear theory. Nonlinear elastic behavior may manifest itself in the generation of harmonics upon dynamic wave propagation, in nonlinear attenuation, resonance frequency shift, and slow time effects. As a first approach (most widely used for the description of nonlinearity in fluids), one generally introduces nonlinearity in the theoretical model by expressing the elastic moduli in a power series of the strain (relative deformation). This is equivalent to accounting for a strain dependency of the energy density at an order higher than the second order (second order corresponds to linear elasticity) [18, 19]. For highly nonlinear materials, even terms of quartic order in strain for the energy density (second order for the moduli) can be considered [30]. However, in most cases, the power series approach is not satisfactory. Highly nonlinear materials exhibit more complicated phenomena in their stress–strain relation. Hysteresis and discrete memory are commonly observed in static tests, and persist even in low-strain dynamic experiments [23–29]. Micro-inhomogeneities such as cracks, voids, and contacts have a complex compliance and the local nonlinear forces may entirely dominate the relatively small atomic nonlinearity. Therefore, the theoretical description of nonlinear mesoscopic elastic materials contains terms that describe classical nonlinearity, as well as hysteresis, and discrete memory [10, 24–29, 31]. To first approximation, the one-dimensional constitutive relation between the stress σ and the strain ε used in simulations of the dynamic behavior of solids can be expressed as follows:

$$\sigma = \int K(\varepsilon, \dot{\varepsilon})\, d\varepsilon, \tag{1a}$$

with K the nonlinear and hysteretic modulus given by

$$K(\varepsilon, \dot{\varepsilon}) = K_0 \left\{1 - \beta\varepsilon - \delta\varepsilon^2 - \alpha[\Delta\varepsilon + \varepsilon(t)\ \mathrm{sign}(\dot{\varepsilon})] + \cdots\right\}, \tag{1b}$$

where K_0 is the linear modulus, $\Delta\varepsilon$ is the local strain amplitude over the previous period [$\Delta\varepsilon = (\varepsilon_{\mathrm{Max}} - \varepsilon_{\mathrm{Min}})/2$ for a simple continuous sine excitation], $\dot{\varepsilon} = d\varepsilon/dt$ is the strain rate, $\mathrm{sign}(\dot{\varepsilon}) = 1$ if $\dot{\varepsilon} > 0$ and $\mathrm{sign}(\dot{\varepsilon}) = -1$ if $\dot{\varepsilon} < 0$ [24, 25, 28, 32]. The parameters β and δ are the classical nonlinear perturbation coefficients, and α is a measure of the material hysteresis.

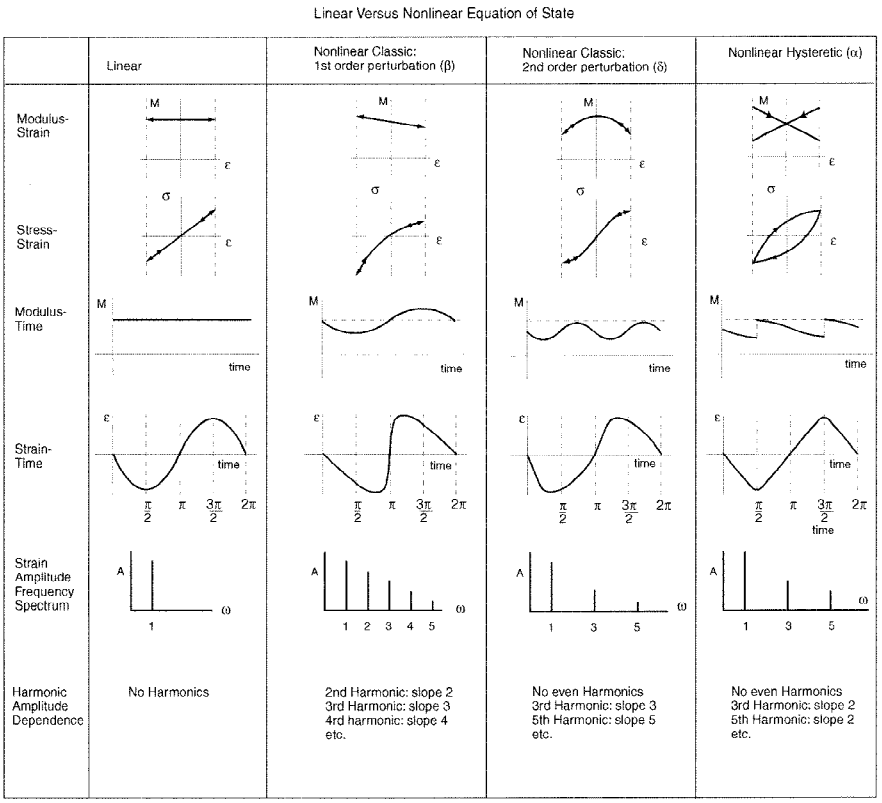

Fig. 1. Schematic overview of the nonlinear contributions to the constitutive equation and its implication for dynamic one-dimensional wave propagation of a finite-amplitude monofrequency signal.

The implication of the nonlinear hysteretic modulus on the acoustic wave propagation is summarized in Fig. 1, where we compare linear wave propagation of a monofrequency signal with the results for the various nonlinear and hysteretic contributions [28]. The figure illustrates the effects on the modulus–strain and stress–strain relation, the deformation of the signal, the harmonic spectrum, and the amplitude dependence of the second and third harmonics. One clearly observes distinct behavior between classical nonlinear and hysteretic nonlinear behavior. It is important to note that the third harmonic for a purely hysteretic material is quadratic in the fundamental strain amplitude, whereas a cubic dependence is predicted by classical nonlinear theory. Analogously, a modulation experiment involving frequencies f_1 and f_2 with amplitudes A_1 and A_2 would result in second-order sideband generation ($f_2 \pm 2\,f_1$) with amplitudes proportional to $\alpha \cdot A_1 \cdot A_2$ in the case of materials with dynamic hysteresis, whereas classical theory would predict a higher-order dependence: $C_{\beta\delta}(A_1)^2 \cdot A_2$, with $C_{\beta\delta}$ a constant combination of β and δ. The first-order intermodulation frequencies at $f_2 \pm f_1$ arise from the classical twofold nonlinear interaction between f_1 and f_2, and their amplitude is proportional to $\beta \cdot A_1 \cdot A_2$.

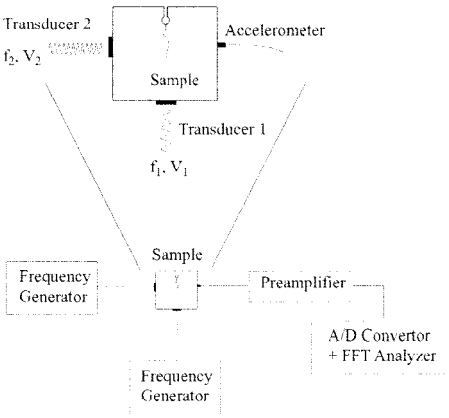

Fig. 2. Sample geometry and experimental configuration for the Plexiglas and sandstone samples.

With this background, we can now move on to the nonlinear wave modulation experiments.

3. Experiment and Configuration

The experimental configuration in applying NWMS is shown in Fig. 2. The Plexiglas and sandstone samples were cut in the manner shown in the figure in order to quantitatively control the cracking of the sample. Cracks were induced by confining the sample center and applying tension to the region of the hole (which had a diameter of 13 mm for both samples). Doing so, we obtained a crack length of 50 mm in the Plexiglas sample with dimensions $110 \times 110 \times 6$ mm, and a crack of 20 mm in the sandstone sample which measured $98 \times 87 \times 18$ mm in dimension. Identical experiments were conducted before and after cracking. In the experiments, two continuous waves with separate frequencies are input into the sample simultaneously using piezoelectric transducers. The first transducer generates a low-frequency signal (typically 5–20 kHz), the second one a high-frequency wave (typically 70–120 kHz). The waves are detected by a calibrated accelerometer at a separate location on the sample. The waveform is preamplified and collected by a 16-bit digitizer, and Fourier analyzed. To illustrate the nonlinear response, one frequency is held at a constant amplitude and the other is stepped up in amplitude from nearly zero to 10 V input. In a sample that is intact (atomic), the output spectrum contains the two frequencies that have been affected by linear processes of wave dissipation and scattering, and by very small atomic nonlinearities. In a sample that is damaged (or nonlinear mesoscopic to begin with), harmonics and sidebands are created by the nonlinearity of the medium in addition to the linear effects. The presence of the harmonics and sidebands indicates microcracking and damage. As explained in the theoretical section, the relationship between the drive amplitudes and the harmonics/sidebands provides clues to the type of nonlinearity of the material.

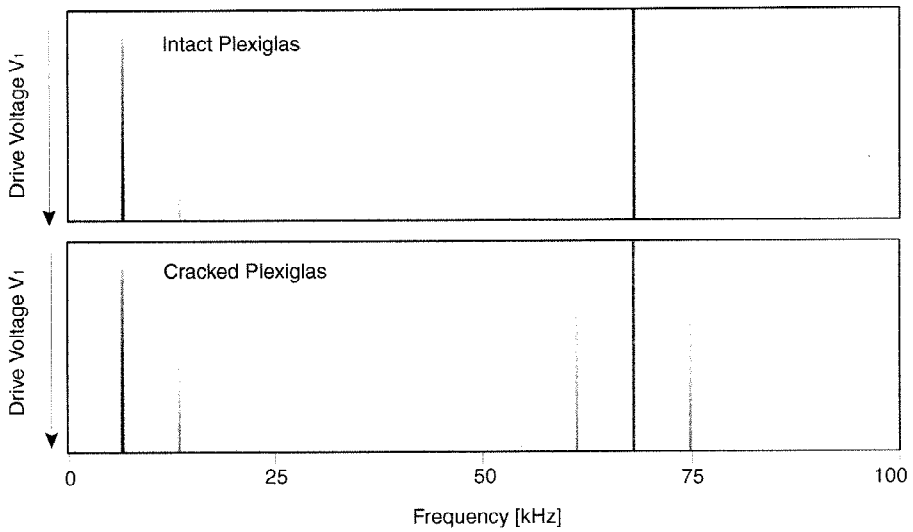

Fig. 3. Interpolated contourplot of the wave modulation spectra ($f_1 = 7$ kHz, $f_2 = 70$ kHz) for an intact and cracked Plexiglas plate in the case of a fixed f_2 drive voltage. The spectral frequency is on the horizontal axis, the f_1 drive voltage (V_1) is on the vertical axis (applied voltage increases downward), and the gray scale corresponds to the measured frequency amplitude (darker tints mean higher amplitudes; the light-gray background corresponds to the noise level). The existence of harmonics and sidebands becomes apparent in the cracked sample.

4. Results

4.1. *Plexiglas*

In the experiment with Plexiglas, the two drive frequencies applied were $f_1 = 7$ and $f_2 = 70$ kHz, respectively. Drive amplitudes for f_1 were 0, 0.1, 0.2, 0.4, 0.8, 1.6, 3.2, 6, and 10 V, respectively, and V_2 was held fixed at a constant voltage. The experiment was performed on an intact sample and on a sample with a 5-cm-long crack. The linear properties of the waveforms, dissipation and wave speed, remained the same in both measurements. Figure 3 illustrates the increasing wave modulation in the measured spectra as a function of the drive amplitude levels for the undamaged and damaged samples, respectively. This figure is an interpolated contourplot with frequency on the horizontal axis, drive voltage V_1 on the vertical axis, and with a gray scale which corresponds to the measured frequency content (darker tints correspond to higher amplitudes; the light-gray background represents the noise floor). There is some amount of harmonic and sideband energy in the intact sample. This is due primarily to nonlinearities in the associated electronics, and a small portion is due to the inherent atomic nonlinearity of the material. In contrast, the damaged sample shows considerably larger harmonics and sidebands.

In order to quantify the relationships between the drive frequencies and the harmonic/modulation signals, we analyzed their dependency on the measured low-frequency am-

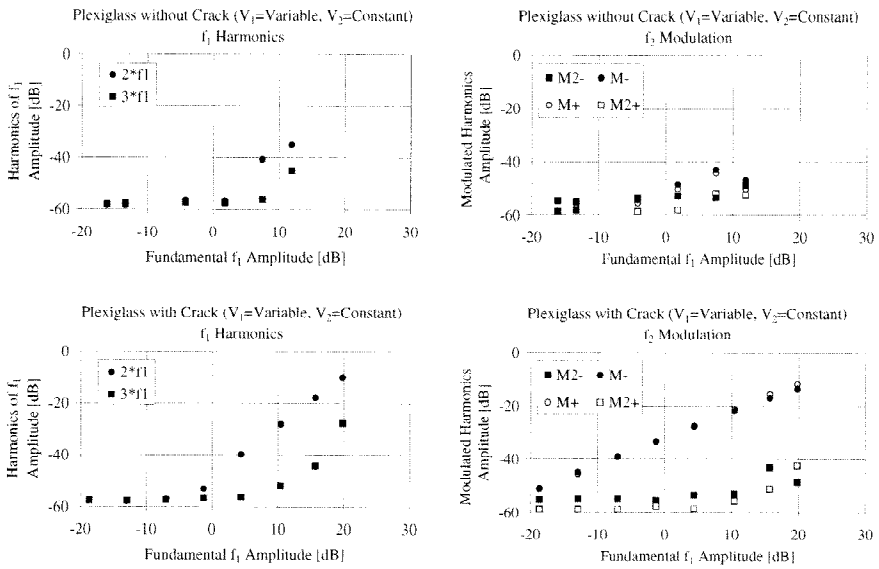

Fig. 4. Analysis of the wave modulation spectra for intact and cracked Plexiglas as a function of the measured fundamental f_1 amplitude: *top*, analysis for the uncracked Plexiglas; *bottom*, analysis for the cracked sample; *left*, harmonics $2f_1$ and $3f_1$; *right*, first and second modulation frequencies $M+$ (at $f_2 + f_1$), $M-$ (at $f_2 - f_1$), $M2+$ (at $f_2 + 2f_1$), $M2-$ (at $f_2 - 2f_1$).

plitude, and plotted them in Fig. 4. It is clear from the intact Plexiglas results shown in the top portion of Fig. 4 that our system noise is of order -40 dB. Above this level we can rely on the observations. The bottom portion of Fig. 4 illustrates the results from the cracked sample. Here we see that the second harmonic $2f_1$ increased in amplitude by at least 20 dB compared to the uncracked sample, and that it has a power-law relation of 2 with the fundamental. This means that the second harmonic has originated by a classical nonlinear twofold frequency interaction between f_1 and itself. The first modulation terms (the actual sum and difference frequencies, indicated by $M+$ and $M-$, respectively) have a slope of 1, which is in agreement with the theoretical prediction. They originate as a result of a first-order interaction between the low- and the high-frequency signal. Compared to the uncracked Plexiglas sample, the level of the first modulation frequencies increased by 20 dB, similar to the increase of the second harmonic. This can only be interpreted as an increase of the classical nonlinearity parameter β with a factor 100. The levels of the third harmonic and of the second modulation terms ($M2+$ and $M2-$ at frequencies $f_2 + 2f_1$ and $f_2 - 2f_1$, respectively) are too small to be analyzed.

4.2. *Sandstone*

We performed a similar experiment on a sandstone sample where the two modulation frequencies applied were $f_1 = 7.9$ and $f_2 = 82.4$ kHz, respectively. This time, we investigated the harmonic and sideband growth as a function of the amplitude of the

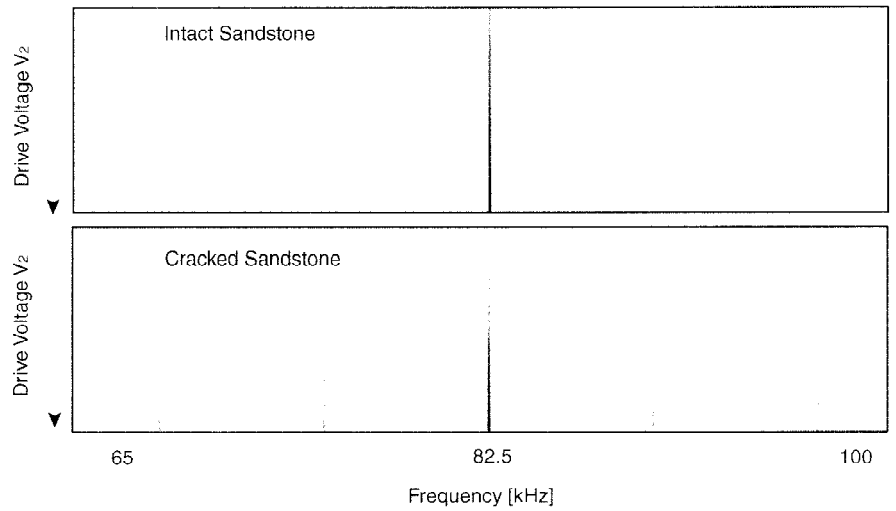

Fig. 5. Similar representation of the wave modulation spectra (limited to the 65–100 kHz band) for uncracked and cracked sandstone as in Fig. 3. In this case V_1 is fixed, and the data are collected for increasing f_2 drive voltage (V_2) (vertical axis, applied voltage increases downward). Again, the existence of sidebands becomes apparent in the cracked sample.

high-frequency signal. The drive amplitudes for f_2 ranged from 0 to 10 V, and V_1 was held fixed at constant voltage. As before, the experiment was performed on an intact sample and on a sample with a 2-cm-long crack. Wave speed and dissipation remained the same in both measurements.

Sandstone is a completely different material than Plexiglas. It is composed of grains bonded together by soft contacts and it generally has numerous microcracks, which makes it nonlinear mesoscopic to begin with. The amplitude-dependent spectra for the uncracked and cracked sandstone sample are illustrated in Fig. 5. Again, the experimental data are shown in an interpolated contourplot with frequency on the horizontal axis, drive voltage V_2 on the vertical axis, and with a gray scale which corresponds to the measured frequency content (darker tints correspond to higher amplitudes). This figure clearly illustrates that an inherently mesoscopic material becomes even more nonlinear when a crack is added.

To quantify the amount of damage, we analyze the dependence of the modulation harmonics on the measured high-frequency amplitude. These are plotted in Fig. 6. The uncracked sample shows a slight appearance of the first modulation frequencies above the noise level of -60 dB. There is no evidence of measurable second-order modulation. The results for the cracked sample, however, show large levels of first and second harmonics (in both sum and difference components). Again, the increase is at least of order 20 dB. Further, we observe that all modulation harmonics have a power-law relation of 1 with the fundamental f_2 amplitude.

In a complementary experiment we fixed the drive amplitude of the high-frequency signal (6 V) and varied the low-frequency component. The analyzed results for the cracked sample are shown in Fig. 7. From the harmonic data, we observe a quadratic de-

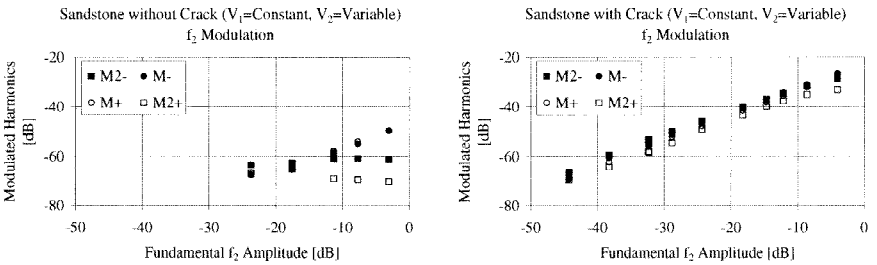

Fig. 6. Analysis of the wave modulation spectra for intact and cracked sandstone as a function of the measured fundamental f_2 amplitude (applied V_1 remains constant): *left*, analysis of the first and second modulation frequencies for the uncracked sandstone; *right*, analysis for the cracked sample.

pendence for both the second and the third harmonic on the fundamental f_1 amplitude. In addition, the modulated components appear to be linear in the low-frequency amplitude. The observations from both experiments combined indicate that the second as well as the third harmonic originate from a twofold f_1 interaction and that both the first and the second modulation sidebands arise from a twofold frequency interaction between f_1 and f_2. However, if classical perturbation theory for nonlinear wave propagation applied, a slope of 3 would be predicted for the third harmonic of f_1, together with a slope of 2 for the second-order modulation terms ($M2+$ and $M2-$) as a function of the f_1. As stated in Section 2, this discrepancy between the classical theory and these experimental results can only be explained by the existence of hysteresis and discrete memory [24–29]. This should be no surprise, however, because we know that all sandstones are mesoscopic nonlinear to begin with.

The conclusion from these observations on sandstone is that, due to the induced damage, both the first-order classical nonlinearity parameter β and the hysteretic parameter α have increased considerably (both the first and the second sideband originate from twofold frequency mixing!), and that the contribution of the third-order nonlinearity represented by the δ term in Eq. (1b) is negligible compared to the contribution of the hysteretic term.

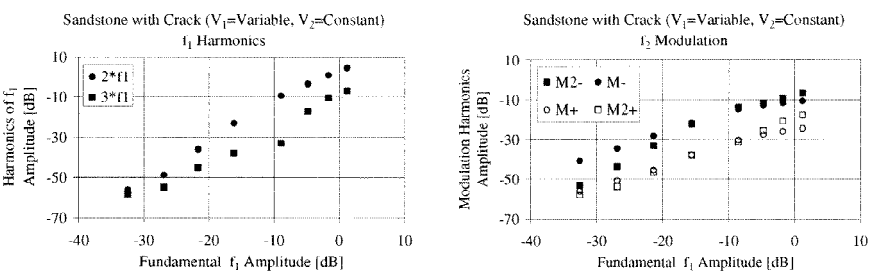

Fig. 7. Analysis of the wave modulation spectra for the cracked sandstone sample as a function of the measured fundamental f_1 amplitude (applied V_2 remains constant at 6 V): *left*, analysis of the harmonics; *right*, analysis of the first and second modulation frequencies.

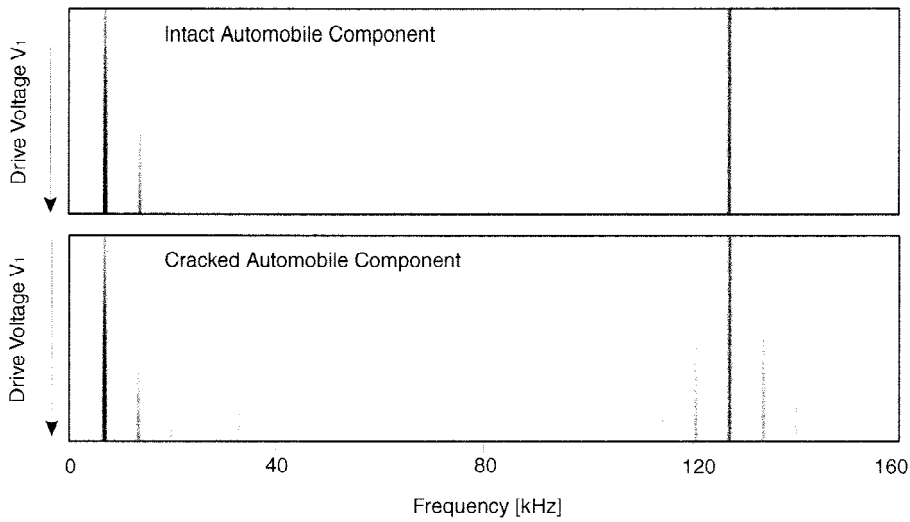

Fig. 8. Interpolated contourplot of the wave modulation spectra for an undamaged and a cracked rocker arm in the case of fixed f_2 drive voltage. Similar representation as in Figs. 3 and 5. The f_1 drive voltage (V_1) is increasing downward on the vertical axis.

4.3. *Automobile Engine Component*

Nonlinear wave modulation experiments have been carried out in materials with complex geometries as well. The tests using complex geometries included those on automobile engine connecting rods, components that are composed of a bar with open circular shapes at each end, much like an elongated number 8. We performed NWMS in two ways: (1) by studying the interaction of two monofrequency continuous wave at various drive voltages of the low-frequency signal (CW-mode NWMS), and (2) by a time-window analysis of the interaction between a high-frequency continuous signal and the entire resonance mode spectrum of the sample, which was excited by tapping the sample with an impact hammer (impact-mode NWMS). Application of both NWMS techniques was successful at discerning an undamaged sample and a sample with a small crack.

In CW mode, the two modulation frequencies applied were $f_1 = 6.7$ and $f_2 = 127.3$ kHz. The drive amplitudes for f_1 were increased in seven intervals to an input level of 10 V. V_2 was held fixed. Figure 8 (again in the form of an interpolated contourplot) shows the amplitude-dependent spectra for the undamaged and cracked connecting rods. The figures clearly illustrate the abundance of harmonics and sidebands in the cracked sample compared to the intact one. This dramatic increase is also visible from Fig. 9, where we plot the level of first- and second-order sum frequencies as a function of the fundamental f_1 amplitude for both the intact and the cracked sample. In the latter, we observe a slope of 1 for the dependence of the first sum frequency component $M+$, and a slope between 1 and 2 for the second-order sum frequency $M2+$. Similar results were obtained for the first- and second-order difference frequencies. This lead to the interpretation that the second-order modulation harmonic originates from a mixed contribution

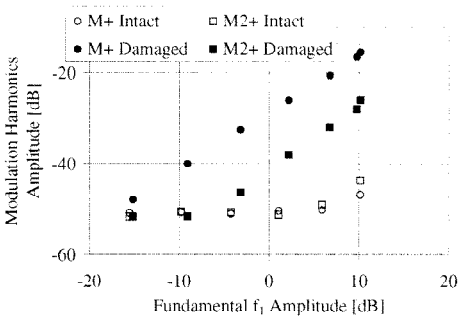

Fig. 9. Analysis of the wave modulation spectra for an intact and a cracked engine part in CW mode. Only the first and second sum frequencies are shown. The difference frequencies show similar behavior.

of classical and hysteretic nonlinear phenomena. The cracked sample definately displays the signs of mesoscopic nonlinearity.

In the impact mode, we tapped the samples with an impact hammer while a high-frequency signal was simultaneously applied to the sample. Due to the impact, all resonance modes are excited. The spectrum is limited in the frequency band to about 20 kHz because of the attenuation of the material. In addition, the low-frequency content generated by the impact lasts for only a limited time, and is attenuated with a characteristic decay time, which is of the order of 100 μs. In order to analyze the nonlinear (or amplitude-dependent) behavior of the samples, we applied a moving time-window analysis to the measured signal by dividing the acquired time record into 6 intervals. Each time window was 10 μs long and contained 4000 data points. A spectral analysis was performed for each of these intervals. The most interesting parts of the modulation spectra are shown in Fig. 10. Even though energy is abundantly present in the low-frequency band, there is no interaction with the high-frequency component for the intact sample. On the other hand, the damaged sample shows large levels of energy in the sidebands, even in the last time window, when the impact energy has nearly disappeared.

The analysis of the wave modulation spectra in the impact-mode NWMS can be performed as follows: (1) define the frequency bands of interest at low frequency (containing all the resonance modes) and similarly around the high-frequency input signal (including all sideband modulations); (2) integrate the power spectrum in the two spectral bands, yielding the "equivalent energy" values I_1 and I_2 for the low and the high frequency, respectively; (3) subtract the "energy" of the f_2 component from I_2; and (4) plot the resulting value against I_1. The outcome of this procedure applied to each time window is shown in Fig. 11, showing the "sideband energy" versus the "impact energy." For the intact unit, we observe a very modest linear increase of the sideband energy with increasing impact energy. In the case of the damaged unit, the dependence has a slope between 1 and 2. The initial growth index (proportionality coefficient of the power law) of this relationship may be used as a damage indicator in quality control, e.g., integrated in a production line.

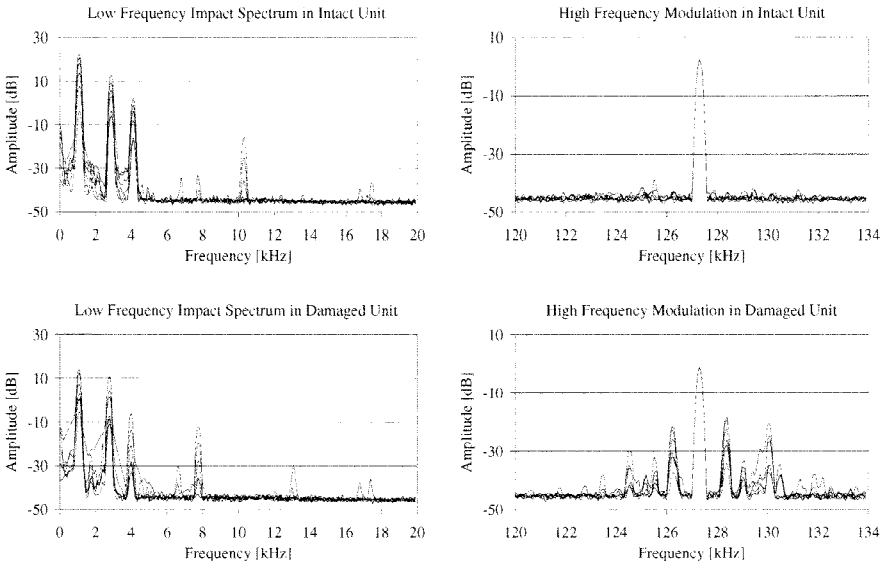

Fig. 10. Low- and high-frequency amplitude spectra in NWMS impact mode (6 levels according to 6 time windows of the acquired wave modulated signal) for an intact and a cracked engine part.

5. Conclusions

The results presented here indicate that the nonlinear response of a material when damaged is extremely large when compared to an intact material. Therefore, acoustic diag-

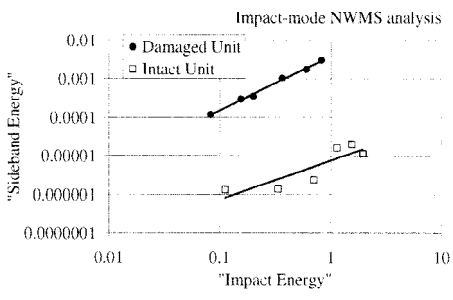

Fig. 11. Integration analysis of the wave modulation spectra for an intact and a cracked engine part in impact mode. Each data point represents the amount of "sideband energy" (integrated high-frequency power spectrum between 120 and 134 kHz, exclusive f_2) in relation to the "impact energy" (integrated low-frequency power spectrum up to 20 kHz) as analyzed from the power spectrum of each of the time windows of the acquired wave modulated signal.

nostic methods that look primarily for nonlinear phenomena such as wave distortion by creation of harmonics and multiplication of waves of different frequencies have a strong potential in damage detection. In undamaged materials, the nonlinear phenomena are very weak. In damaged materials, they are remarkably large. Because of the complex (i.e., nonlinear and hysteretic) compliance of cracks and flaws, the sensitivity of nonlinear methods to the detection of damage features is far greater than that of any linear acoustical methods.

The method outlined in this paper focused on the nonlinear interaction of low- and high-frequency signals. The method is fast and efficient, and proved to be very effective in discerning an undamaged sample and a sample with a small crack. It can be applied to any type of geometry, and may therefore possess a huge potential in large-scale applications involving nonlinear studies; monitoring reactor containment walls for damage, inspecting aircraft and spacecraft, observing fatigue damage in buildings, bridges, tunnels, gas and oil pipelines, quality control in assembly lines, etc.

Acknowledgments. This research has been financed by a research grant of the Flemish Institute for the promotion of scientific and technological research in the industry (IWT, Brussels, Belgium); by the Research Council of the Catholic University of Leuven, Belgium; by the Office of Basic Energy Research, Engineering and Geoscience (contract W-7405-ENG-36); and by a University Collaborative Research Program of The Institute of Geophysics and Planetary Physics at Los Alamos National Laboratory, NM, USA.

References

1. O. Buck, W. L. Morris, and J. N. Richardson. *Appl. Phys. Lett.* **33**(5):371 (1978).
2. M. Richardson. *Int. J. Eng. Sci.* **17**:73 (1979).
3. W. L. Morris, O. Buck, and R. V. Inman. *J. Appl. Phys.* **50**(11):6737 (1979).
4. P. B. Nagy. *Ultrasonics* **36**:375 (1998).
5. P. B. Nagy, P. McGowan, and L. Adler. *Rev. Prog. QNDE* **10B**:1685 (1990).
6. L. Adler and P. B. Nagy. *Rev. Prog. QNDE* **10B**:1813 (1991).
7. P. B. Nagy and L. Adler. *Rev. Prog. QNDE* **11**:2025 (1992).
8. W. T. Yost and J. H. Cantrell. *Rev. Prog. QNDE* **9B**:1669 (1990).
9. J. H. Cantrell and W. T. Yost. *Phil. Mag.* **A69**:315 (1994).
10. V. E. Nazarov, L. A. Ostrovskii, I. A. Soustova and A. M. Sutin. *Sov. Phys. Acoust.* **34**:284 (1988).
11. V. A. Antonets, D. M. Donskoy, and A. M. Sutin. *Mech. Composite Mater.* **15**:934 (1986).
12. A. M. Sutin, C. Declos, and M. Lenclud. In *Proc. 2nd Symp. Acoustical and Vibratory Surveillance Methods and Diagnostic Techniques*, Senlis, France, p. 725 (1995).
13. A. M. Sutin and D. M. Donskoy. *Proc. SPIE* **3397**:226 (1998).
14. P. A. Johnson, B. Zinszner, and P. N. J. Rasolofosaon. *J. Geophys. Res.* 11553 (1996).
15. K. Van Den Abeele and J. A. TenCate. Submitted for publication (1999).
16. L. W. Byers, J. A. TenCate, G. Guthrie, W. Carrie, and P. A. Johnson. *J. Cement and Concrete*, in review (1999).
17. K. Van Den Abeele, J. Carmeliet, J. A. TenCate, and P. A. Johnson. This issue.
18. M. F. Hamilton. In *Nonlinear Wave Propagation in Mechanics*, **AMD-77**. The American Society of Mechanical Engineers, New York (1986).
19. L. D. Landau and E. M. Lifshitz. *Theory of Elasticity*. Pergamon, Tarrytown, NY (1959).
20. V. E. Nazarov and A. M. Sutin. *J. Acoust. Soc. Am.* **102**(6):3349 (1997).
21. K. Naugolnykh and L. Ostrovsky. *Nonlinear Wave Processes in Acoustics*. Cambridge Texts in Applied

Mathematematics, Cambridge University Press (1998).
22. A. M. Sutin and V. E. Nazarov. *Radiophys. Quantum Electron.* **38**(3–4):109 (1995).
23. P. A. Johnson and R. A. Guyer. *Phys. Today* (April 1999).
24. K. R. McCall and R. A. Guyer. *J. Geophys. Res.* **99**:23887 (1994).
25. K. R. McCall and R. A. Guyer. *Nonlinear Proc. Geophys.* **3**:89 (1996).
26. R. A. Guyer, K. R. McCall, and G. N. Boitnott. *Phys. Rev. Lett.* **74**:3491 (1994).
27. V. E. Nazarov. *Akust. Ah.* **43**:225 (1997) [English transl.: *Acoust. Phys.* **43**:192 (1997)].
28. K. Van Den Abeele, P. A. Johnson, R. A. Guyer, and K. R. McCall. *J. Acoust. Soc. Am.* **101**(4):1885 (1997).
29. V. E. Gusev, W. Lauriks, and J. Thoen. *J. Acoust. Soc. Am.* **103**(5):3216 (1998).
30. K. Van Den Abeele. *J. Acoust. Soc. Am.* **99**(6):3334 (1996).
31. V. E. Nazarov, L. A. Ostrovsky, I. A. Soustova, and A. M. Sutin. *Phys. Earth Planet. Interiors* **50**:65 (1988).
32. R. A. Guyer, K. R. McCall, and K. Van Den Abeele. *Geophys. Res. Lett.* **25**:1585 (1998).